

Low-field NMR studies of  
polymer crystallization kinetics:  
changes in the melt dynamics

C. Hertlein<sup>1</sup>, K.Saalwächter<sup>2</sup> and G. Strobl<sup>1</sup>

<sup>1</sup>Physikalisches Institut

Albert-Ludwigs-Universität

79104 Freiburg, Germany

<sup>2</sup>Fachbereich Physik

Martin-Luther-Universität Halle-Wittenberg

06108 Halle/Saale, Germany

**Abstract**

The free induction decay in <sup>1</sup>H NMR experiments carried out for crystallizing polymers can be directly decomposed in contributions from crystals, melt-like regions and amorphous regions with a reduced mobility. Here the results of time-dependent experiments conducted with the aid of a cost-efficient low-field NMR instrument are presented, obtained for sPP, P $\epsilon$ CL and P(EcO). Crystallization isotherms are compared with those obtained by X-ray scattering and dilatometry. There are some minor systematic deviations which can be explained and accounted for. For all systems a large fraction of amorphous chain parts in regions with a reduced mobility is found.

# 1 Introduction

Being sensitive to the segmental mobility, NMR experiments are used since long time as one of the tools which provide an analysis of the different states of order which coexist in semi-crystalline polymers [1][2][3]. Commonly,  $^1\text{H}$ -NMR is employed when the experimental time is an important issue, and it has the advantage of being very sensitive to molecular mobility. The signals obtained here in the frequency or time domain generally represent a superposition of at least three components, associated with protons within the crystallites, in melt-like regions and in amorphous regions with a reduced mobility. In the majority of cases NMR is applied to quiescent samples, where structural changes arising from variations in the conditions of solidification are investigated. However, as only a short time is required for the registration of a signal, NMR is also a convenient tool for time-dependent investigations, hence in particular, for studies of the kinetics of polymer crystallization.

Bridges et al. [4] were the first ones using measurements of the free induction decay (FID) for this purpose. The decay is usually completed within 100 ms, and a longitudinal relaxation time of usually around or less than a second allows a high repetition rate. Noting that the transverse magnetization of the protons within crystallites decays within  $32 \mu\text{s}$ , whereas a much longer time is required for all the other ones, Bridges et al and later also Cohen-Addad and coworkers [5][6][7] used this initial drop in the signal amplitude for a determination of the crystallinity. Crystallization isotherms then followed from time-dependent experiments at a fixed temperature. In more recent experiments Kristiansen et al. [8][9][10] focussed at a full formal decomposition of the FID signals registered during the crystallization of polyethylene. Convenient analytical representations were chosen for assumed four different components, and the decomposition was carried out by standard least-square fitting techniques. Such approaches are also favored by Litvinov [11][12], who established the use of a cost-efficient low-field NMR instrument for a phase composition analysis in quiescent samples. In this work, we set out to test the use of such

an equipment to monitor polymer crystallization kinetics, while using a method for FID signal decomposition that is not dependent on model assumptions.

During the last years we investigated the crystallization properties of several polymers - s-poly(propylene) (sPP), poly(ethylene-co-octene) (PEcO), poly( $\epsilon$ -caprolactone) (P $\epsilon$ CL) [13], i-poly(styrene) [14], and poly(L-lactide) [15] - by X-ray scattering, dilatometry and DSC. Results indicate a multistage process during the growth of polymer crystallites with a passage through a transient mesomorphic phase [16]. In an attempt to further broaden the experimental basis we now employed also NMR in studies of the crystallization kinetics. Experiments were carried out for sPP, PEcO and P $\epsilon$ CL, in each case for one sample. We compared the NMR data with the crystallization isotherms obtained in the former investigations.

## 2 Experimental Section

### 2.1 Samples

The sample of P $\epsilon$ CL was produced by Sigma-Aldrich Co and has a molar mass  $M_w = 5.6 \cdot 10^4$  g mol<sup>-1</sup>. The sample of sPP was supplied by FINA; the molar mass is  $6.6 \cdot 10^4$  g mol<sup>-1</sup>. The sample of PEcO, obtained from Dow Chemicals, has 14% per weight of octene units and a molar mass  $M_w = 3 \cdot 10^4$  g mol<sup>-1</sup>.

In order to remove all memory effects the samples were at first heated outside of the NMR spectrometer to a temperature far above their respective melting points [17]. From there, they were rapidly transferred into the spectrometer whose heating chamber was preset to the chosen crystallization temperature  $T_c$ . The cooling of the sample to  $T_c$  required about 2 minutes. We set the zero time of the experiment to the time at which  $T_c$  was reached.

## 2.2 NMR Spectroscopy

A 0.5-T Bruker minispec mq20 low-resolution NMR spectrometer (19.9 MHz proton Larmor frequency) was used for the experiments reported herein. The polymer samples were molten to cover the bottom 5 mm of 8 mm OD sample tubes that were placed in the center of the rf coil for good rf homogeneity. While the minispec offers a bore that holds 10 mm OD sample tubes, the use of centered 8 mm tubes lead to better (but still far from satisfactory, see below) temperature reproducibility, probably due to a more even airflow around the sample. The average sample temperature was calibrated using an external thermometer.

The minispec provides  $90^\circ$  pulses of less than  $2 \mu\text{s}$  length and a fast digitizer, yet the dead time of about  $12 \mu\text{s}$  precludes a precise quantification of solid components that are considerably dephased on this timescale by the multiple strong dipolar couplings. This problem may be solved by a dedicated equipment with extremely short dead time [8], but is more commonly addressed by help of a solid echo, where many experiments with variable echo delays and an extrapolation have to be performed; a solid echo cannot fully refocus multiple dipolar couplings in a dense proton system (see [11][12] for recent applications of this approach).

As such an extrapolation procedure is prohibitive for fast real-time applications, we here employ the pulsed version of the mixed magic-sandwich echo (MSE) [18][19], which forms a full multi-spin dipolar and chemical-shift echo after a total delay of  $76 \mu\text{s}$  and thus removes the necessity for extrapolation. This will be detailed in an upcoming publication [20], where we show that its implementation on the minispec serves to almost quantitatively refocus the proton magnetization and thus allows one to detect the complete sample magnetization as the intensity at the echo top. After sampling the refocused FID for  $90 \mu\text{s}$  (with a dwell time of  $1 \mu\text{s}$ ), we appended a Carr-Purcell-Meiboom-Gill (CPMG) echo pulse train [21][22] with an  $180^\circ$  pulse spacing of  $200 \mu\text{s}$ , where the first pulse is centered  $32 \mu\text{s}$  after the last digitized point. Further points are then acquired on every echo top. As the full-phase signal is acquired in

absorption mode, there is no need for a more elaborate phase cycling within the pulse train. The CPMG train serves to refocus chemical-shift and susceptibility effects, and a quick pulse succession is advantageous to obtain a good time resolution (with a minimized decay during the first echo) and also to suppress relaxation effects that are associated with the dynamics in local field gradients, e.g. around voids [23].

We can therefore safely assume that the remaining decay is mainly associated with effects of dipolar-mediated relaxation due to intermediate to slow timescale dynamics in the amorphous parts as well as residual dipolar couplings that arise from non-isotropic motions of entangled and tethered chains [24]. It is thus expected to depend on the local morphology of the sample. In our upcoming publication [20], these conceptual issues, along with details on a different extrapolation procedure used to obtain the crystallinity, will be dealt with in detail. In the following, we focus on a model-free decomposition of the amorphous decay as well as on the comparison of NMR results with those of other methods.

### 3 Results and Discussion

At first, the data obtained for P $\epsilon$ CL are presented and they are used to explain our evaluation procedure. Then, the results obtained for sPP and PEcO are shown and discussed.

#### 3.1 Poly( $\epsilon$ -caprolactone)

Figure 1 displays the FIDs which were recorded when P $\epsilon$ CL crystallized at 50 °C . The uppermost curves are those obtained at the beginning when the sample is still in the molten state, and the lowest curves are those measured at the end when the crystallization process is completed. One observes a continuous change in the curve shape. The main feature is the development of a first rapid decay of the FID amplitude completed at about 32  $\mu$ s. The decay is to be associated with protons in the crystallites which experience strong dipole-dipole interactions. The FID

measurement ends at around 0.5 s; then the amplitude of the FID signal has dropped to vanishingly small values. Note the negligible decay of the initial intensity for  $\tau \rightarrow 0$ , that essentially proves the success of the MSE to fully refocus the crystalline signal. The major drawback of the minispec as compared to high-field equipment is the noise level, which is about one order of magnitude higher. Consequently, the very early stages of crystallization are not well accessible.

The log-log representation of the FIDs shows that in the asymptotic limit of long decay times one finds always the signal of the melt, reduced in intensity. This behavior suggests as a first step in the data evaluation an elimination of the melt-like component. This can be achieved by an adjustment of the FID of the melt to the curve measured at some crystallization time which can be accomplished choosing an appropriate reduction factor. This reduction factor directly yields the mass fraction of protons which are at this crystallization time still in melt-like surroundings, and we denote it  $\phi_{\text{ma}}$ . The term ‘melt-like’ refers here to the local mobility only. It does not mean that the overall state of motion of these protons is identical with that in the melt; the presence of crystallites can affect the motion in the fluid parts everywhere.

The signal which remains after a subtraction of the melt-like component is to be assigned to all protons which have changed their local mobility, i.e. both, those included in the crystals and those which are in amorphous regions in the vicinity of crystal surfaces. Figure 2 shows these signals, denoted  $A_r(\tau)$ , throughout the crystallization process. Each curve shows the rapid initial decay assigned to crystalline protons followed by a slower decay completed at about 10 ms. The simplest procedure for a decomposition in the two parts is that suggested by Bridges et al and Cohen-Addad et al: One uses the signal drop until  $32 \mu\text{s}$ , i.e., at the break, as yielding a measure of the fraction of protons included in crystallites, here denoted  $\phi_c$ . The remaining part is that originating from protons with a reduced mobility in amorphous surroundings. In the literature the region of the latter is sometimes addressed as ‘rigid-amorphous’, and we denote the corresponding fraction  $\phi_{\text{ra}}$ . Note that this nomenclature deviates somewhat from common

practice, as the intermediate fraction is often extracted via a three (or more) component fit, and may be characterized by a decay time on the order of  $100 \mu\text{s}$  [11].

Figure 3 shows as the result of the data evaluation the three fractions as a function of time, i.e.,  $\phi_c(t)$ ,  $\phi_{\text{ma}}(t)$ ,  $\phi_{\text{ra}}(t)$ . All three fractions change simultaneously in correlated manner. According to the evaluation, the crystallinity would reach a final value of 0.57. The larger part of the amorphous phase has a reduced mobility due to the presence of the crystallites, amounting to  $\phi_{\text{ra}} = 0.33$ . Only 10% of the material remains in the melt-like state.

In contrast to the NMR analysis, X-ray scattering experiments and dilatometry cannot distinguish between the rigid-amorphous and the melt-like amorphous phase, since the two regions have the same density. One can, however, compare the development of the crystallinity with time. Figure 4 depicts data obtained for the same sample in dilatometric measurements and by crystallinity determinations employing small angle X-ray scattering (from [25]). Both measurements yielded for the final crystallinity a value of 0.42, which is significantly below the NMR result.

A second difference shows up in the kinetics. The transition from the initial range with an increase according to  $\phi \sim t^\nu$  (here we have  $\nu=4$ ) to the final value as represented in the log-log plot is definitely sharper in the isotherm obtained by X-ray scattering and dilatometry than in the curves  $\phi_c(t)$  obtained by NMR. There is one obvious reason for the deviation of the NMR result for the final crystallinity, and it is indicated in Fig. 5: Choosing the signal value after the initial drop for a determination of  $\phi_c$  implies a neglect of a possible drop of the signal assigned to the rigid-amorphous component within the first  $32 \mu\text{s}$ . If one tentatively chooses the continuation as is indicated in Fig. 5, the value of  $\phi_c$  is reduced. If one secondly considers that NMR yields the mass fraction while X-ray scattering gives the volume fraction crystallinity, the at first quite large deviation of the NMR result practically vanishes. However, since there is no basis for a theoretical description of the FID of the protons in the rigid amorphous phase, the

extrapolation to zero time remains purely empirical. Under such conditions we prefer using the at least well-defined procedure of Bridges, being aware that the crystallinities thus obtained are somewhat too large.

The smoothing of the transition of the NMR isotherms from the initial increase to the final range when compared with the dilatometric and X-ray scattering curves is due to a temperature gradient in the sample within the heating stage of the NMR spectrometer. For the device in use, a temperature distribution with a width of about 3 °C was indicated in a measurement of the clearing point of a liquid crystal (that is detected as a change in  $T_2$ ). Figure 6 shows, based on the measured dilatometric curves obtained for sharp temperature values, the curves to be expected for such a temperature gradient, and they indeed agree with those measured in the NMR spectrometer. This constitutes a serious problem for precise kinetics experiments with the minispec. The temperature gradient can certainly be reduced, however, this would have required a construction of a dedicated heating device, which we did not embark on for this orientation study. As we noted, the problem did not arise for a 500 MHz high-field spectrometer using a commercial static double-tuned probe.

### 3.2 s-Poly(propylene)

Figure 7 displays FIDs which were measured during the crystallization of sPP at  $T_c = 110$  °C . The melt-like part has already been subtracted in the above described manner. The curves  $A_r(\tau)$  thus show again the development of the signal produced by all protons with a reduced mobility. It increases with time. Again one can differentiate between protons incorporated in crystals which contribute that part in the signal which drops to zero within 32  $\mu$ s, and the remaining part which needs 10 ms for the total decay. The latter ones are protons in the rigid-amorphous phase. The simple procedure for a separation, referring to the value of  $A_r$  at 32  $\mu$ s, yields a crystallinity  $\phi_c = 0.25$ . Here  $\phi_c$  is below the value associated with the rigid-amorphous phase

which amounts to  $\phi_{\text{ra}} = 0.38$ . The melt-like regions occupy at the end about 37% of the sample. The time dependence of the fractions of the three different regions is shown in Fig. 8. As in the case of P $\varepsilon$ CL all three phases develop simultaneously, i.e., the half-times of transition agree with each other.

Again, the crystallinity value obtained in the simple manner is somewhat too large, as is shown by a comparison with the results of analogous measurements in the dilatometer or by X-ray scattering. Both yielded a value  $\phi_c = 0.20$  [25]. The reason for the deviation is the same one as in the case of P $\varepsilon$ CL: The FID of the protons in the rigid-amorphous phase changes between  $\tau = 32\mu\text{s}$  and  $\tau = 0$ . In view of this effect one can say, that the NMR results agree with the other measurements.

### 3.3 Poly(ethylene-co-octene)

In the case of PEcO the FIDs associated with protons with a restricted mobility have the appearance shown in Fig. 9. It is obvious that here the fraction of crystallites remains very small until the end. In spite of that, there exists a large region where the mobility of the chain sequences is reduced. The largest part of the sample remains melt-like, also when the crystallization process is finished. Figure 10 depicts the development with time of  $\phi_c$ ,  $\phi_{\text{ma}}$  and  $\phi_{\text{ra}}$ . Again, the amplitude of  $A_r$  at  $\tau = 32\mu\text{s}$  was used for a determination of the crystallinity. It leads here to a final crystallinity of about 10%, which essentially agrees with dilatometric and X-ray results [26].

### 3.4 Resumé

Figure 11 presents at the end all the measured crystallization isotherms  $\phi_c(t)$  in a comparison. The NMR results give the correct sequence for both, the final values of the crystallinity with the largest value for P $\varepsilon$ CL and the smallest for PEcO, and also for the initial slopes, again with the

largest values for P $\epsilon$ CL and the smallest one for PEcO. Hence, employing NMR in studies of the crystallization kinetics of polymers gives basically correct results and yields, in addition to the conventional tools dilatometry and X-ray scattering, valuable information on the mobility reductions in non-crystalline regions. On the other hand, one has to be aware of perturbing factors, which can introduce systematic errors, not too large but non-negligible ones.

In principle, the peculiar properties of NMR allow also a detection of ordering phenomena prior to the formation of crystals. In the experiments described here we could not find such features. As a matter of fact, this is not surprising, because the sensitivity of the NMR experiments, being comparable to the other conventional tools, does not allow to pick up the initial stages of the crystallization process. Observations begin only when the growing spherulites are already well developed.

### Acknowledgements

R. Mülhaupt, Institut für Makromolekulare Chemie, Freiburg, is thanked for the use of the minispec. Support of this work by the Deutsche Forschungsgemeinschaft is gratefully acknowledged. Thanks are also due to the 'Fonds der Chemischen Industrie' for the generous financial help provided over many years.

### References

- [1] K. Bergmann. *J.Polym.Sci.-Polym.Physics*, 16:1611, 1978.
- [2] R. Kitamaru and F. Horii. *Adv.Polym.Sci.*, 26:137, 1978.
- [3] R. Kitamaru, F. Horii, and K. Murayama. *Macromolecules*, 19:636, 1986.
- [4] B. J. Bridges, A. Charlesby, and R. Folland. *Proc. R. Soc. Lond. A*, 367:343, 1979.

- [5] G. Feio and J. P. Cohen-Addad. *J. Polym. Sci. B Polym. Phys.*, 26:389–412, 1988.
- [6] G. Feio, G. Buntinx, and J. P. Cohen-Addad. *J. Polym. Sci. B Polym. Phys.*, 27:1–24, 1989.
- [7] R. H. Ebengou and J. P. Cohen-Addad. *Polymer*, 35:2962, 1994.
- [8] E. W. Hansen, P. E. Kristiansen, and B. Pedersen. *J. Chem. Phys. B*, 102:5444–5450, 1998.
- [9] P. E. Kristiansen, E. W. Hansen, and B. Pedersen. *J. Phys. Chem.*, 103:3552, 1999.
- [10] P. E. Kristiansen, E. W. Hansen, and B. Pedersen. *Polymer*, 42:1969, 2001.
- [11] V. M. Litvinov and J. P. Penning. *Macromol. Chem. Phys.*, 205:1721–1734, 2004.
- [12] V. M. Litvinov and M. Soliman. *Polymer*, 46:3077–3089, 2005.
- [13] B. Heck, T. Hugel, M. Iijima, E. Sadiku, and G. Strobl. *New J. Physics*, 1:17, 1999.
- [14] M. Al-Hussein and G. Strobl. *Macromolecules*, 35:1672, 2002.
- [15] T.Y. Cho and G. Strobl. *Polymer*, 47:1036, 2006.
- [16] G. Strobl. *Eur. Phys. J. E*, 18:295, 2005.
- [17] B. Heck and G. Strobl. *Colloid Polym Sci*, 282:5117, 2004.
- [18] W.-K. Rhim, A. Pines, and J. S. Waugh. *Phys. Rev. B*, 3:684696, 1971.
- [19] S. Matsui. *Chem. Phys. Lett.*, 179:187–190, 1991.
- [20] A. Maus, C. Hertlein, K. Saalwächter, and G. Strobl, submitted.
- [21] H. Y. Carr and E. M. Purcell. *Phys. Rev.*, 94:630–638, 1954.
- [22] S. Meiboom and D. Gill. *Rev. Sci. Instrum.*, 29:688–691, 1958.
- [23] D. Geschke and G. Fleischer. *Acta Polym.*, 42:362–366, 1991.

- [24] J. P. Cohen-Addad. *Progr. NMR Spectrosc.*, 25:1–316, 1993.
- [25] G. Strobl. *Progr. Polym. Sci.*, in press, 2006.
- [26] A. Häfele, B. Heck, T. Hippler, T. Kawai, P. Kohn, and G. Strobl. *Eur. Phys. J. E*, 16:207, 2005.

## Figures

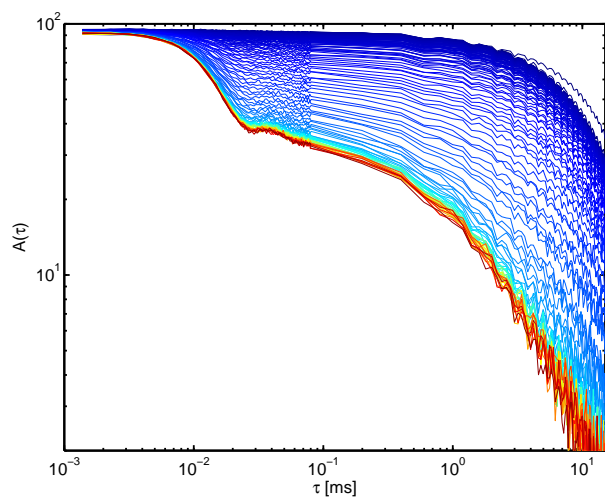


Figure 1: P $\epsilon$ CL, crystallization at 50 °C studied by  $t$ -dependent  $^1\text{H}$  NMR. FID signals  $A(\tau)$  recorded during the crystallization process

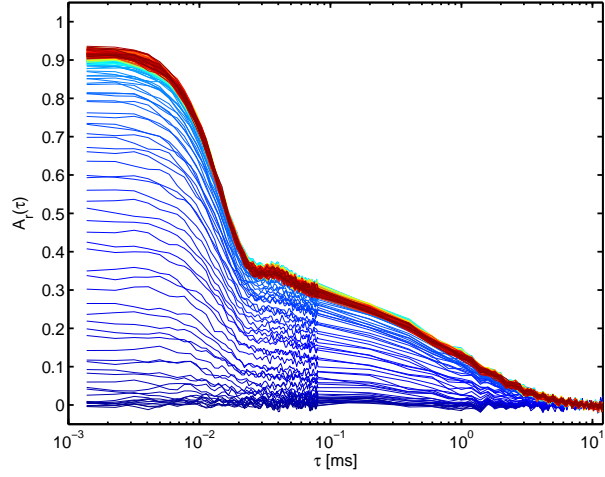


Figure 2: P $\epsilon$ CL, crystallization at 50 °C : Part  $A_r(\tau)$  in the FIDs contributed by protons with a reduced mobility. It is obtained by an elimination of the contribution of protons with a melt-like mobility from the FIDs in Fig.1

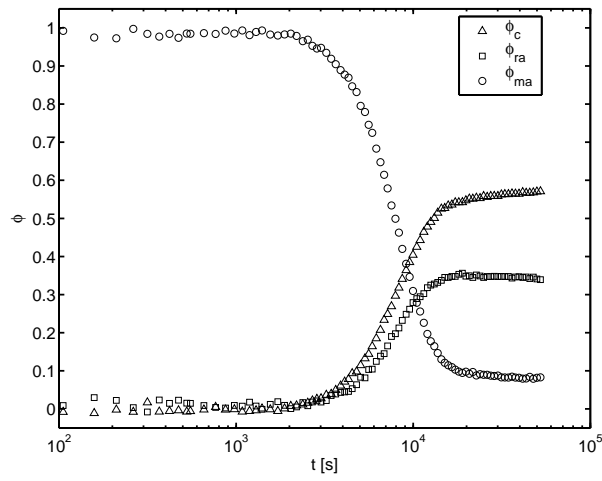


Figure 3: P $\epsilon$ CL, crystallization at 50 °C , evaluation of the FIDs: Time dependence of the mass fractions of protons in crystals ( $\phi_c$ ), in amorphous regions with a reduced mobility ( $\phi_{ra}$ ), and in melt-like regions ( $\phi_{ma}$ ), respectively

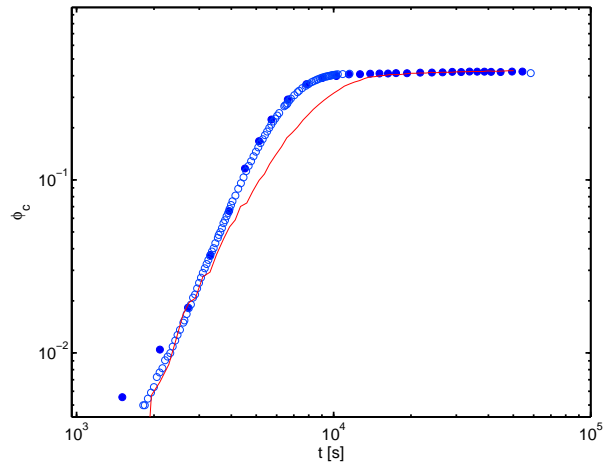


Figure 4: P $\epsilon$ CL, crystallization at 50 °C : Isotherms obtained by X-ray scattering (*filled circles*) and dilatometry (*open circles*). Comparison with the NMR result ( $\phi_c(t)$  in Fig.3 adjusted to the final dilatometric crystallinity)

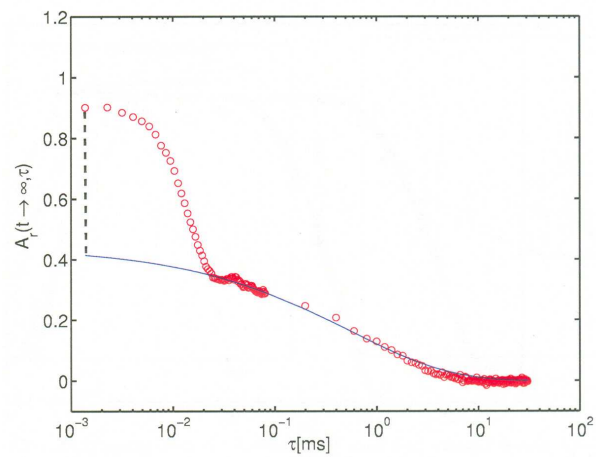


Figure 5: P $\epsilon$ CL, crystallized at 50 °C , FID of the protons with reduced mobility: Tentative continuation of the part associated with amorphous regions leading to a correct crystallinity value

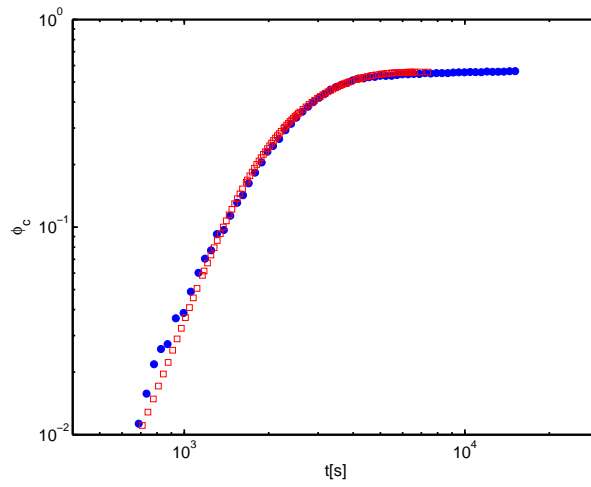


Figure 6: Simulation (*circles*) of the NMR result (*filled circles*) assuming a temperature distribution with a width of 3 °C within the sample

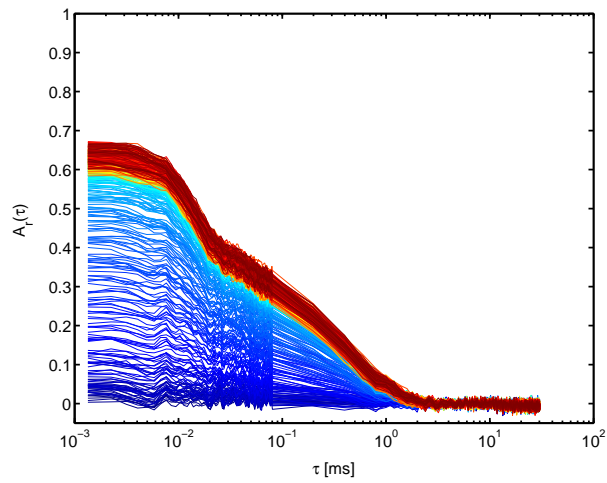


Figure 7: sPP, crystallization at 110 °C : FIDs associated with all protons with a reduced mobility

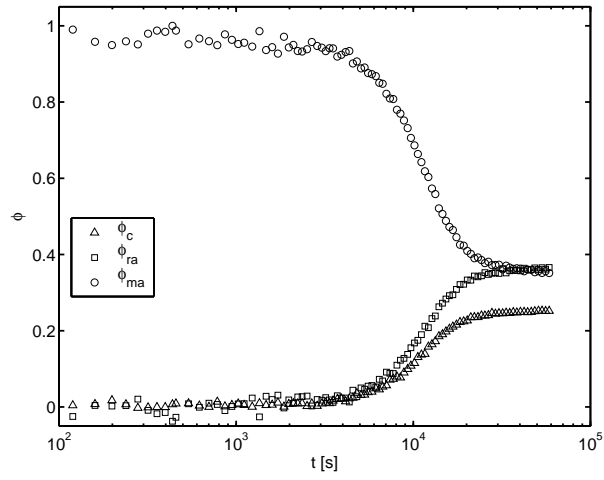


Figure 8: sPP, crystallization at 110 °C , evaluation of the FIDs : Time dependence of the mass fractions of protons in crystals ( $\phi_c$ ), in amorphous regions with a reduced mobility ( $\phi_{ra}$ ), and in melt-like regions ( $\phi_{ma}$ ), respectively

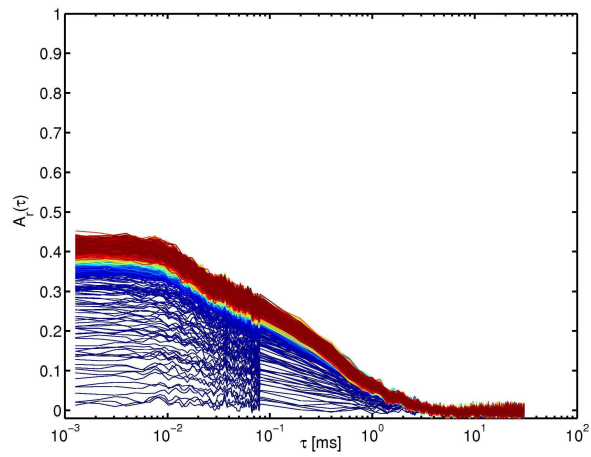


Figure 9: PEcO, crystallization at 91 °C : FIDs associated with all protons with reduced mobility

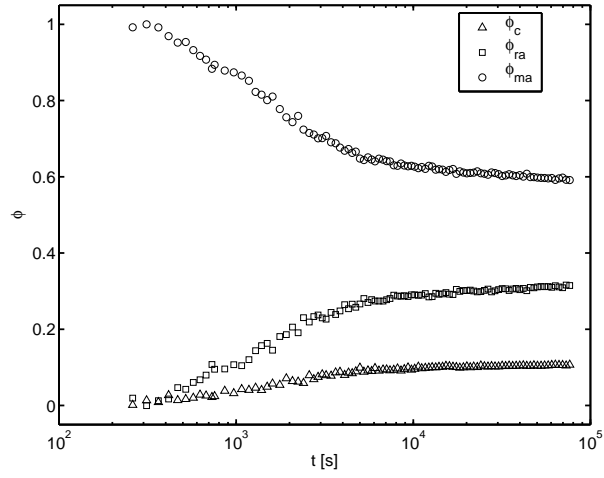


Figure 10: PEO, crystallization at 91 °C , evaluation of the FIDs : Time dependence of the mass fractions of protons in crystals ( $\phi_c$ ), in amorphous regions with a reduced mobility ( $\phi_{ra}$ ), and in melt-like regions ( $\phi_{ma}$ ), respectively

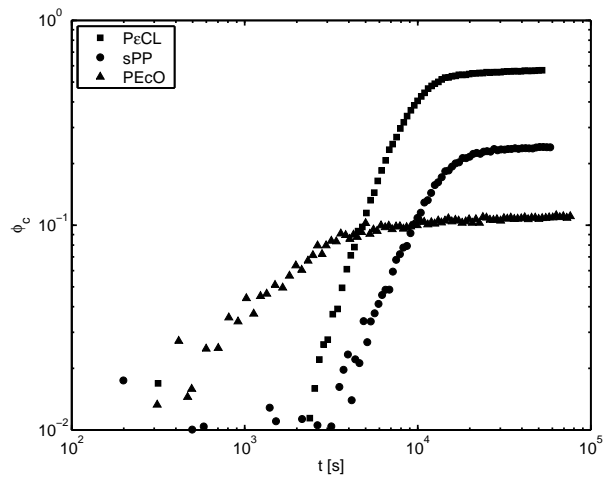


Figure 11: Comparison of the isotherms  $\phi_c(t)$  obtained for the three samples